Macromolecular Research

Article

DOI 10.1007/s13233-022-0045-5

www.springer.com/13233 pISSN 1598-5032 eISSN 2092-7673

# Mechanical, Thermal, and Rheological Properties of Phlogopite-Incorporated Polycarbonate and Polystyrene

Sang-Seok Yoon[†,1]
Sung-Hun Lee[†,1]
Gyu-Chul Hwang[2]
Min-Kyu Choi[1]
Beom-Goo Kang[3]
Hyungsu Kim[4]
Keon-Soo Jang*[,1]

[1] Department of Polymer Engineering, School of Chemical and Materials Engineering, The University of Suwon, Hwaseong, Gyeonggi 18323, Korea
[2] SKC Co., ltd., Suwon, Gyeonggi 16338, Korea
[3] Department of Chemical Engineering, Soongsil University, Seoul 06978, Korea
[4] Department of Chemical Engineering, Dankook University, Yongin, Gyeonggi 16890, Korea

Received November 9, 2021 / Revised February 16, 2022 / Accepted February 18, 2022

**Abstract:** Polymer/phlogopite composites have been rarely investigated despite their potential applications. We examined the effects of phlogopite on the mechanical, thermal, and rheological properties of two amorphous polymers, namely, ductile polycarbonate (PC) and brittle polystyrene (PS). The mechanical and thermal properties of PS/phlogopite composites improved with increasing phlogopite content. The modulus of PC/phlogopite composites showed a greater increase as a function of phlogopite concentration probably due to the good interfacial attraction between the phlogopite and PC, compared with the other filler-embedded PC composites. The mechanical and thermal properties (except for the modulus of PC/phlogopite composites) decreased owing to the PC chain scission (reduction in molecular weight) during extrusion, which was caused by the phlogopite infiltration into the PC matrix. The phlogopite's effects on the abovementioned polymers were compared with those on other fillers such as kaolin and silica.

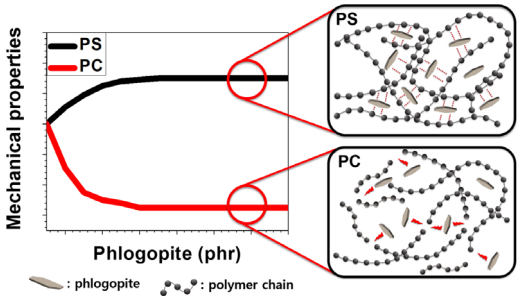


**Keywords:** phlogopite, polycarbonate, polystyrene, mechanical properties, thermal properties.

## 1. Introduction

Among amorphous polymers, polycarbonate (PC) and polystyrene (PS) are representatives of ductile and brittle polymers, respectively. PC features the transparency, flame-retardancy, and an excellent balance of mechanical, physical, thermal and electrical properties due to the combination of phenyl and carbonate moieties.[1-3] However, PC has some drawbacks such as hydrolysis at high temperature and humidity, low chemical-resistance, and high coefficient of thermal expansion.[4] PS has transparency, good processability, and mechanical properties but has poor durability, wear resistance, and chemical resistance.[5-7] Therefore, PC and PS have been widely compounded with inorganic fillers such as silica, talc, mica, glass fiber, $CaCO_3$, ZnO, and carbon-based fillers (carbon nanotube, graphene, etc) to compensate for the weak points of PS and PC.[7-9] As an example, the incorporation of modified silane-functionalized silica into PC and PS enhanced the thermal and mechanical properties of the composite.[10,11] PC and PS were also compounded with metal oxide nanoparticles to improve mechanical, thermal, optical, electrical and flame-retardant properties, and dimensional stability.[7,12,13]

In particular, mica is commonly utilized to enhance various properties including electrical insulation and adiabatic properties of polymers.[14] For instance, the incorporation of mica into the PC matrix solved drawbacks, such as hydrolysis, low chemical resistance, and high coefficient of thermal expansion.[15-18] In addition, the durability, wear resistance, and chemical resistance of mica-reinforced PS composites can be enhanced.[14,19,20] A recent interest in phlogopite (derivative of mica: $KMg_3(Al, Si)_4O_{10}(OH, F)_2$) has surfaced because it is easily broken, elastic, soft, hard to dissolve, and heat-resistant, compared with other mica-related fillers. Phlogopite can be translucent or opaque, depending on the thickness. Its Mohs hardness, specific gravity Temperature of decomposition are 2.5-3.0, 2.76-2.90, and 800-1000 ℃, respectively.[14,21] For instance, phlogopite has been added into polyethylene and polypropylene to improve mechanical properties.[22,23] In this study, we systematically examined the effect of phlogopite on various properties of the brittle (PS) and ductile (PC) polymers in comparison with silica and kaolin.

## 2. Experimental

### 2.1. Materials

Low and high molecular weight (MW) PCs (PC-1220R and Infino-1100R) were supplied by Lotte Chemical Co. (South Korea). The melt flow index (MFI) of low and high MW PCs was 22 and 10 g/10 min (300 ℃/1.2 kg), respectively. PS (Styroution PS 147F) was obtained from BASF Co. (Germany); its MFI was 6.5 g/10 min under the condition of 200 ℃/5.0 kg. Phlogopite, silica, and kaolin were supplied by LKAB Minerals Co. (Sweden), 3M Co. (Saint Paul, MN, USA), and DaOne Chemical Co. (South Korea), respectively.

***Corresponding Author:** Keon-Soo Jang (ksjang@suwon.ac.kr)
[†]S.-S. Yoon and S.-H. Lee contributed equally; Co-1st authors.

### 2.2. Composite fabrication processing extrusion and injection

Each polymer was dried at 100 ℃ for 3 h to remove moisture prior to extrusion and then phlogopite and polymers were mixed by using a tumbler mixer for 10 min. The pre-mixed mixture was extruded via an intermeshing co-rotating twin-screw extruder (STS25-44V-SF, Hankook EM Ltd., South Korea). The screw diameter, length-to-diameter (L/D) ratio, and die hole diameter were 25, 44, and 4 mm, respectively. The screw rotational speed, feeding rate, barrel temperatures, and die temperature were 60 rpm, 1.5 kg/h, 180-240 ℃ for PC (100-200 ℃ for PS), and 210 ℃ for PC (180 ℃ for PS), respectively. All components were simultaneously fed into the extruder hopper (100 ℃) vertically. The vacuum pressure in barrels was 0.90 MPa. The extrudates from the die were cooled in a water bath at room temperature and subsequently pelletized. Three kneading sections are designed as shown in Figure 1.

The extruded composite pellets were dried at 60 ℃ for 24 h to remove residual moisture prior to injection molding process. Specimens for property tests such as tensile test, Izod impact strength test, and rheological test were prepared by an injection molding machine (LGH50N, LS Mtron Co., South Korea). The screw diameter, injection pressure, cooling time were 25 mm, 98 MPa, and 15 s, respectively. The barrel temperatures for PC and PS were 260-280 ℃ and 200-220 ℃, respectively, and the mold temperature was 20-24 ℃ (room temperature).

### 2.3. Characterization

#### 2.3.1. Scanning electron microscopy

The morphologies of phlogopite/PC and phlogopite/PS composites were observed by scanning electron microscopy (SEM; Apro, FEI Co., USA) at an electron beam voltage of 10.0 kV and magnification of ×1000. The fractured specimens for SEM examination were obtained from the Izod impact strength tests. The fractured surface was coated with a 5-10 nm thick gold layer by using a sputter coater prior to the SEM measurements.

#### 2.3.2. Differential scanning calorimetry

Differential scanning calorimetry (DSC; DSC85, TA Instruments., USA) was performed to obtain the melting ($T_m$) and glass transition temperatures ($T_g$) of polymers and composites. Approximately 2-3 mg of samples were placed in a hermetic aluminum pan and heated at a scanning rate of 10 ℃/min under nitrogen purging (50 mL/min). The second heating cycle was utilized to report the transition temperatures.

#### 2.3.3. Dynamic mechanical analysis

Dynamic mechanical analysis (DMA; Discovery DMA 850, TA Instruments., USA) was conducted in a tensile mode. Rectangular specimens (dimensions: approximately 35 mm long, 10 mm wide, and 4 mm thick) were prepared to measure the storage and loss moduli, and $T_g$. The $T_g$ values of samples were determined based by the peak points of tan $\delta$. The measurements were performed at a single frequency of 1 Hz and a constant amplitude of 20 μm. The heating rate was 3 ℃/min.

#### 2.3.4. Tensile test

Uniaxial tensile deformation was utilized on the universal tensing machine (UTM; LR10K Plus, LLOYD instruments., United Kingdom). The tests were performed according to ISO 527. The specimen cross-section had dimensions of 10 mm × 4 mm and the gauge length was 80 mm. The specimens were elongated at a constant cross head speed of 50 mm/min at room temperature. The mean values were determined based on five specimens.

#### 2.3.5. Izod impact strength test

Notched Izod impact strength tests (43-02 Monitor Impact Tester, Testing Machines Inc., USA) were performed according to ISO 180 with rectangular dimensions of 4.0 mm × 10 mm × 80 mm. The notch depth, radius, and angle of specimens were 2 mm, 0.25±0.5 mm, and 45°, respectively. The radius of the hammer knife edge was 0.8 mm and the hammer lift angle was 150°. The hammer velocity at the moment of impact was 3.5 m/s. The capacity of the tester was 150 kgf/cm. The mean values were determined among seven specimens for each sample.

#### 2.3.6. Melt flow index measurement

Melt flow index (MFI) was measured by an MFI machine (WL1400SA, Withlab Co., South Korea) on the standard test method, KS M3070 and ISO E1133. The dimensions of the standard die orifice (nozzle) were 2.095 mm × 8 mm. The piston diameter was 9.5 mm. The samples were dried at 100 ℃ for 3 h prior to the measurements. The measurement temperature was 220 ℃ with a load of 2.16 kg for PC and 230 ℃ with a load of 2.16 kg for PS, respectively. The pellets were inserted into the piston, and the samples were pre-heated for 5 min.

#### 2.3.7. Thermogravimetric analysis

Thermogravimetric analysis (TGA; Perkin Elmer Co., USA) was performed according to ISO 11358. The samples with mass of 1.0-1.2 mg were heated from 30 to 500 ℃ at a heating rate of 10 ℃/min. The samples were held at 500 ℃ for 1 h. The $N_2$ gas

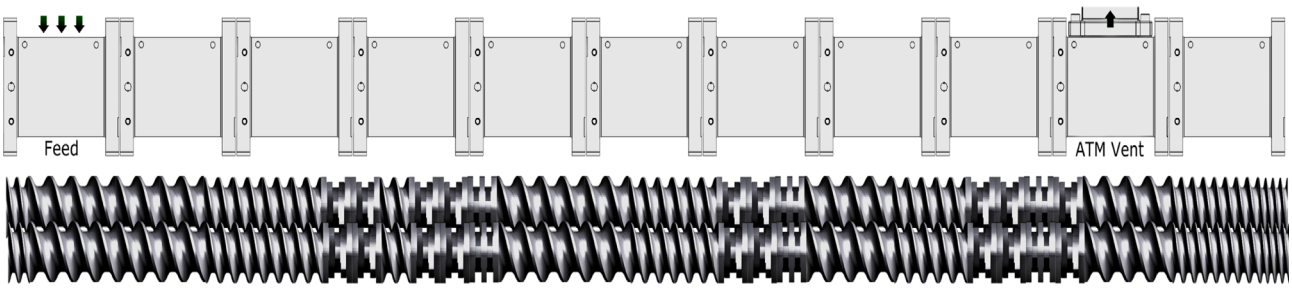


**Figure 1.** Modular screw configuration for co-rotating twin-screw extruder.

was purged at a gas flow of 20.0 mL/min at gas pressure of 2.2 bar.

### 2.3.8. Fourier transform infrared spectroscopy

Fourier transform infrared (FTIR, Nicolet 6700, Thermo Fisher Scientific Co., USA) spectroscopy was performed in the attenuated total reflection (ATR) mode to detect C-O bonds. The sample was dissolved in tetrahydrofuran and filtered to remove the fillers. Subsequently, the solution was dried and the film-shaped sample was measured. Each FTIR spectrum was recorded in a wavenumber region of 2500-500 $cm^{-1}$ by conducting 16 scans.

### 2.3.9. Gel permeation chromatography

The molecular weight of PC and PS was determined by GPC. Each polymer and composite was 0.1 wt% dissolved in Tetrahydrofuran 99.9% (THF, HPLC Grade, Samchun Co., South Korea). The resulting solution was filtered via the PTFE syringe filter (Hydrophobic PTFE syringe filter 0.22 μm Futecs Co., South Korea). The filtered solution was injected to the three GPC columns (5, 3, and 0.5 μm) at an injection speed of 1 mL/min.

## 3. Results and discussions

Visual observation for polymer/mineral filler composites has been routinely investigated by SEM. Figures 2, 3, S1, and S2 show the morphologies of L-PC/P, H-PC/P, and PS/P composites with different phlogopite concentrations. The fractured surfaces of pristine PC were smooth, whereas those of pristine PS showed the curved morphology. The number of phlogopite in the composite increased as a function of phlogopite concentration. The platy morphology of phlogopite was maintained after extrusion. The phlogopite fillers were homogenously dispersed within the PC and PS matrices. As the phlogopite content increased, the curved morphology was more obvious.

The mechanical properties of mineral filler/polymer composites are the most important among various properties such as mechanical, thermal, rheological, electrical, and optical properties. Stress-strain curves for the composites are shown in Figure S3. The tensile strength (Figure 4(a)) and elongation at break (Figure 4(b)) of PS/P composites increased up to PS/P5 and decreased above 5 phr with increasing phlogopite concentration, whereas those of L-PC/P and H-PC/P composites decreased down to 10-20 phr of phlogopite and then slightly increased beyond this value. The effects of filler on strengths are based on two factors: (1) Positive and (2) negative factors compete. Stress is dispersed from the matrix to fillers, which have higher strength. However, at high filler concentrations, the stress is concentrated on the matrix, thereby resulting in debonding between the matrix and filler.[24]

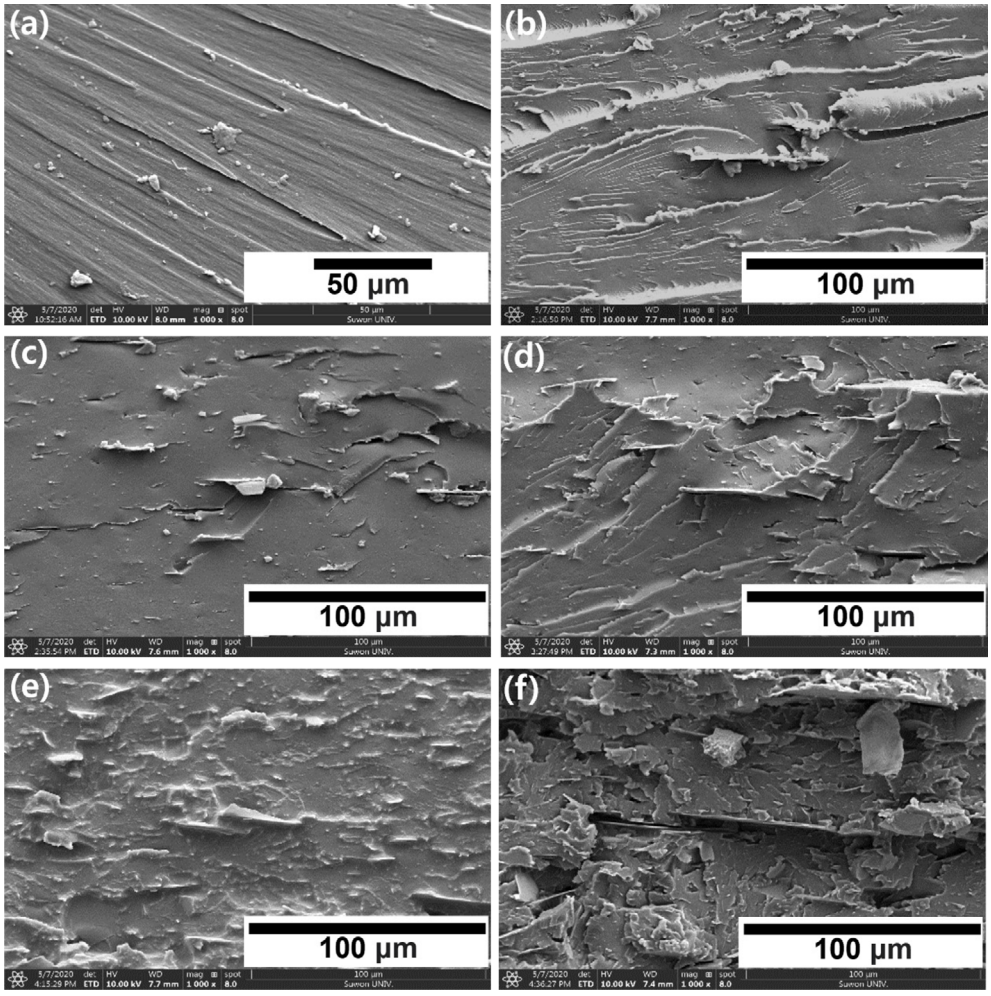


**Figure 2.** SEM images of pure L-PC and L-PC/P composites with different phlogopite concentrations: (a) Pure L-PC, (b) L-PC/P2.5, (c) L-PC/P5, (d) L-PC/P10, (e) L-PC/P20, and (f) L-PC/P30.

 

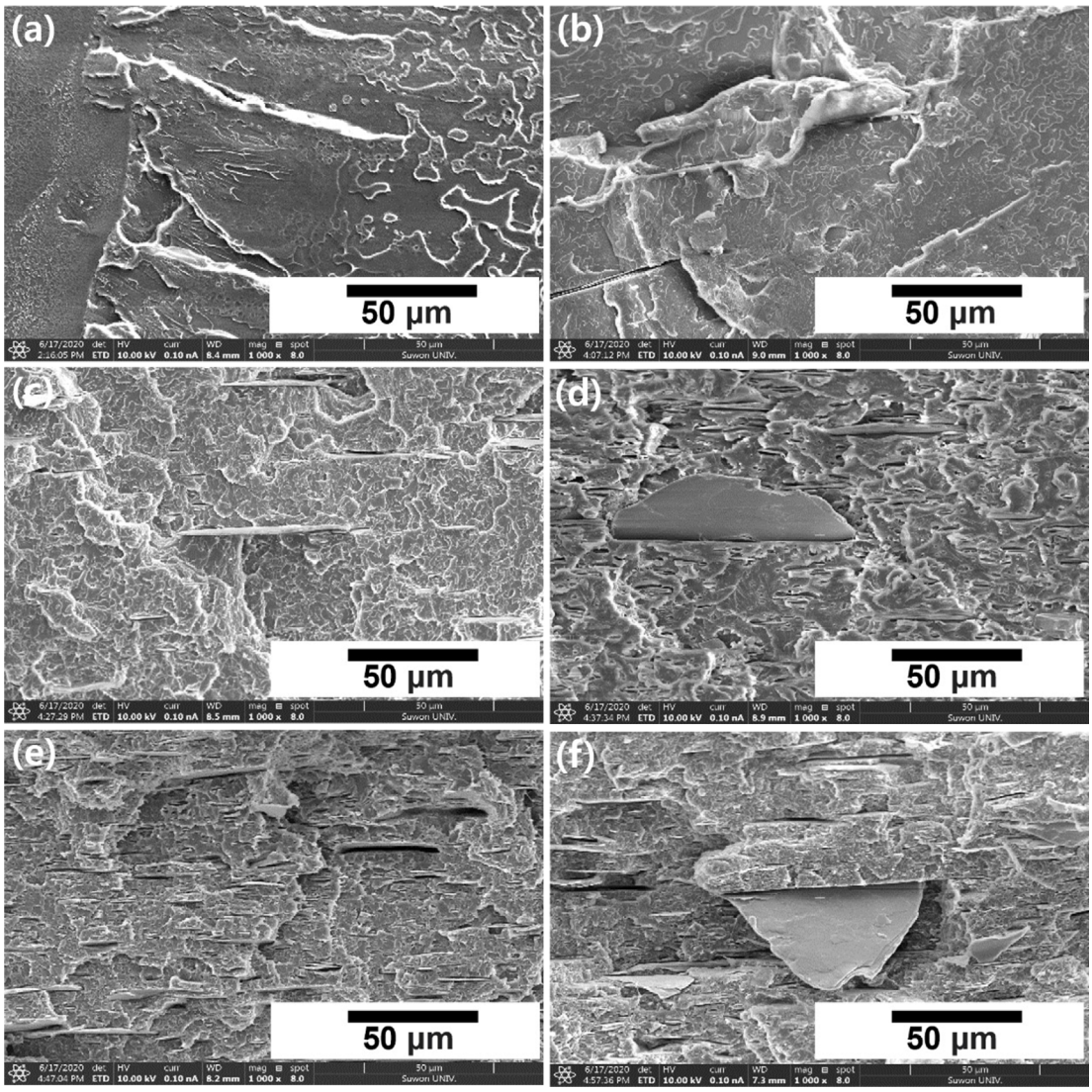


**Figure 3.** SEM images of pure PS and PS/P composites with different phlogopite concentrations: (a) Pure PS, (b) PS/P2.5, (c) PS/P5, (d) PS/P10, (e) PS/P20, and (f) PS/P30.

In addition, the PC chains are susceptible to the bond cleavage due to the filler (phlogopite), thereby reducing the chain length of molecules and resulting in brittleness. PC is degraded to bisphenol A with the yellowing issue and reduction in viscosity.[25-30] The PC chains are also thermally cleaved (pyrolysis).[31-35]

When the PC matrix became brittle, the incorporation of phlogopite increased the tensile strength and elongation at break of the composites. Figure 4(c) shows that the tensile moduli of the three composites (L-PC/P, H-PC/P, and PS/P) gradually increased as a function of phlogopite content because the fillers carried out stresses between the loaded filler and matrix by an elastic matrix-rigid filler mechanism.[24] Thus, the strength and modulus increased until some limiting content and halted the increase, depending on the adhesion between the filler and polymeric matrix. The strength decreased because of filler-induced brittleness which resulted in low elongation at break. The modulus which was determined at the initial stage during elongation typically increased substantially as a function of filler concentration. These findings are in good agreement with the Einstein-Guth-Gold equation (Eq. (1)).[36,37]

$$E = E_0 (1 + 2.5\phi + 14.1\phi^2) \quad (1)$$

$$E = E_0 (1 + 0.67\alpha\phi + 1.62\alpha\phi^2) \quad (2)$$

where $E$ and $E_0$ are the tensile moduli of the composites and pure polymeric matrix, respectively. $\phi$ and $\alpha$ are the filler volume fraction and aspect ratio, respectively.

The Einstein-Guth-Gold equation is involved with spherical fillers-embedded polymer composites, whereas the modified Einstein-Guth-Gold equation (Eq. (2)) predicts the modulus of fibrous fillers-incorporated polymer composites with factors ($\alpha$) of filler shape.[38] The major and minor axises of elliptic phlogopite were determined to be 39.4 ± 27.2 μm and 30.5 ± 25.6 μm, respectively, based on SEM images (Figure S4). The aspect ratio (major axis/minor axis) was 1.54. The Young's moduli of L-PC/P, H-PC/P and PS/P composites obtained by the experimental measurements were analogous to those determined by the Eqs. (1) and (2) until 10 phr phlogopite (Figure 5). Above 10 phr, the experimental results were close to the modified Einstein-Guth-Gold equation (Eq. (2)) rather than the Einstein-Guth-Gold equation (Eq. (1)).

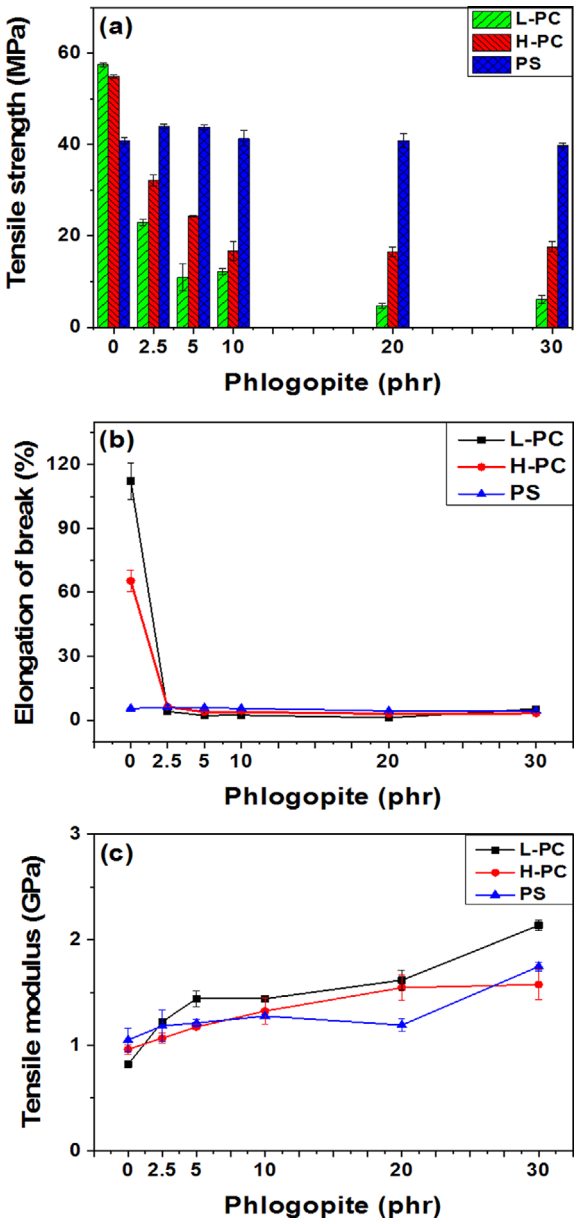


**Figure 4.** Mechanical properties of phlogopite-incorporated L-PC, H-PC, and PS composites with different phlogopite contents: (a) tensile strength, (b) elongation at break, and (c) tensile modulus.

In addition to tensile tests, the Izod impact strength test was performed to examine the effect of phlogopite on the PC and PS matrices. The incorporation of even low filler loadings into PC matrices typically brings about the ductile-to-brittle transition since the high-modulus mineral fillers act as a stress concentration within the PC matrix.[39] Thus, the infiltration of phlogopite into low molecular weight and high molecular weight PCs dramatically reduced the impact strength of composites. In addition, the phlogopite might have resulted in the PC chain scission during extrusion, thereby decreasing the MW of PC. In contrast, the impact strength of PS/P composites slightly increased because PS had the brittle characteristics and thus the stress transfer mechanism was dominant over the stress concentration phenomenon. In addition, the phlogopite might have not cleaved the PS chains unlike the PC chains. The change in MW of PS and PC will be discussed.

Viscoelastic (storage and loss moduli, the associated tan $\delta$, $T_g$, and sub-$T_g$ molecular motions; $\beta$ and $\gamma$ relaxations), mechanical, and thermal properties of polymers are characterized by DMA. In particular, DMA is the most accurate method to determine a $T_g$ of a polymer. Variations in modulus at a certain frequency occur as a function of temperature because of changes in cooperative motions among various molecular motions such as divergent localized or medium-long range cooperative motions of molecular segments. $T_g$ can be determined by three viscoelastic parameters of DMA, namely, $E'$ onset, $E''$ peak, and tan $\delta$, which contribute to mechanical failure, physical property change, and systematical change with amorphous content, respectively. The storage moduli of the three composite series (L-PC/P, H-PC/P, and PS/P) increased with increasing phlogopite content owing to the elastic properties of phlogopite and stress transfer mechanism between the filler and matrix (Figure 6). The incorporation of phlogopite into the PC matrix reduced the $T_g$ values of the PC composites (L-PC/P and H-PC/P) probably because of the PC chain scission as shown in Table 1. In contrast, the $T_g$ values of PS/P composites slightly increased as a function of phlogopite concentration, indicating no chain scission occurring during extrusion. The $T_g$ values determined by storage and loss moduli (DMA) agreed well with those obtained by DSC as shown in Table 1 and Figures 7, 8, 9, and S5. The loss moduli (energy dissipated as heat) of the composites (L-PC/P, H-PC/P, and PS/P)

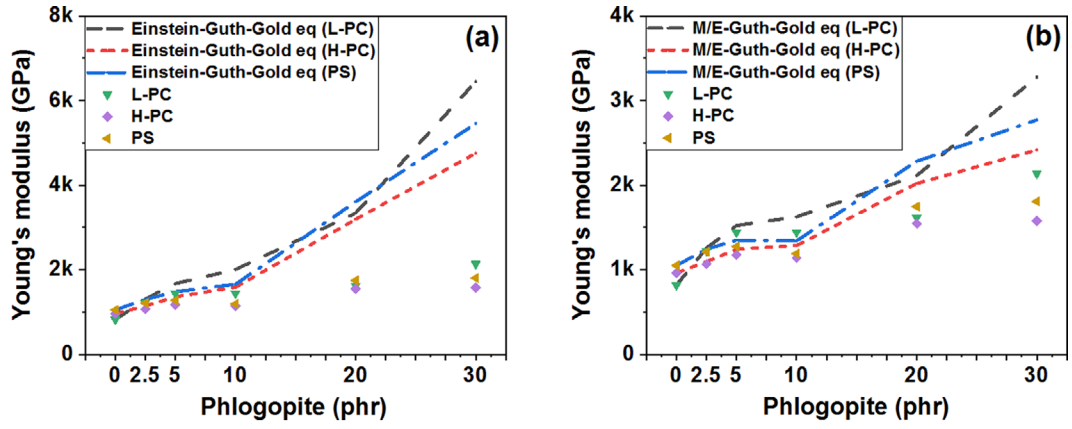


**Figure 5.** Comparison between experimental and theoretical results (a) Einstein-Guth-Gold equation, (b) Modified Einstein-Guth-Gold equation of phlogopite-incorporated L-PC, H-PC, and PS composites with different phlogopite contents.

 

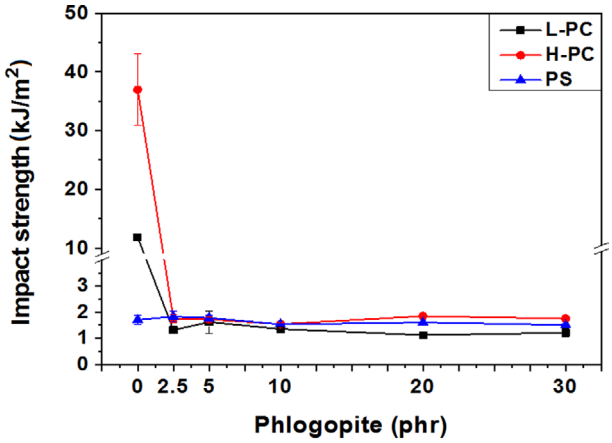


**Figure 6.** Impact strength of phlogopite-incorporated L-PC, H-PC, and PS composites with different phlogopite contents.

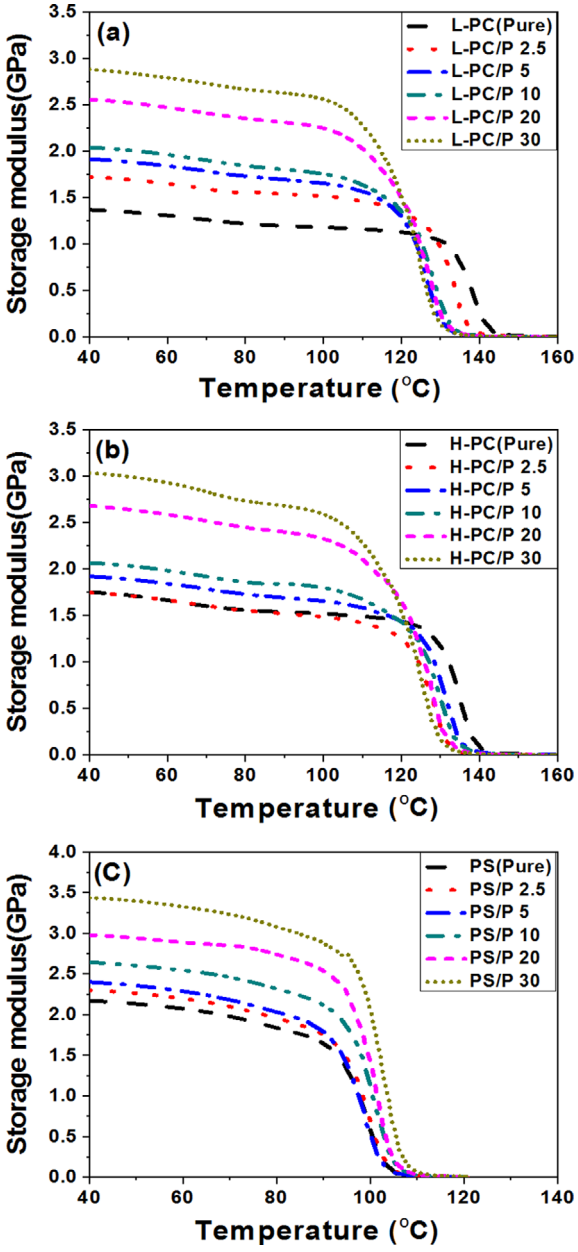


**Figure 7.** Storage moduli of phlogopite-incorporated (a) L-PC, (b) H-PC, and (c) PS composites with different phlogopite loadings.

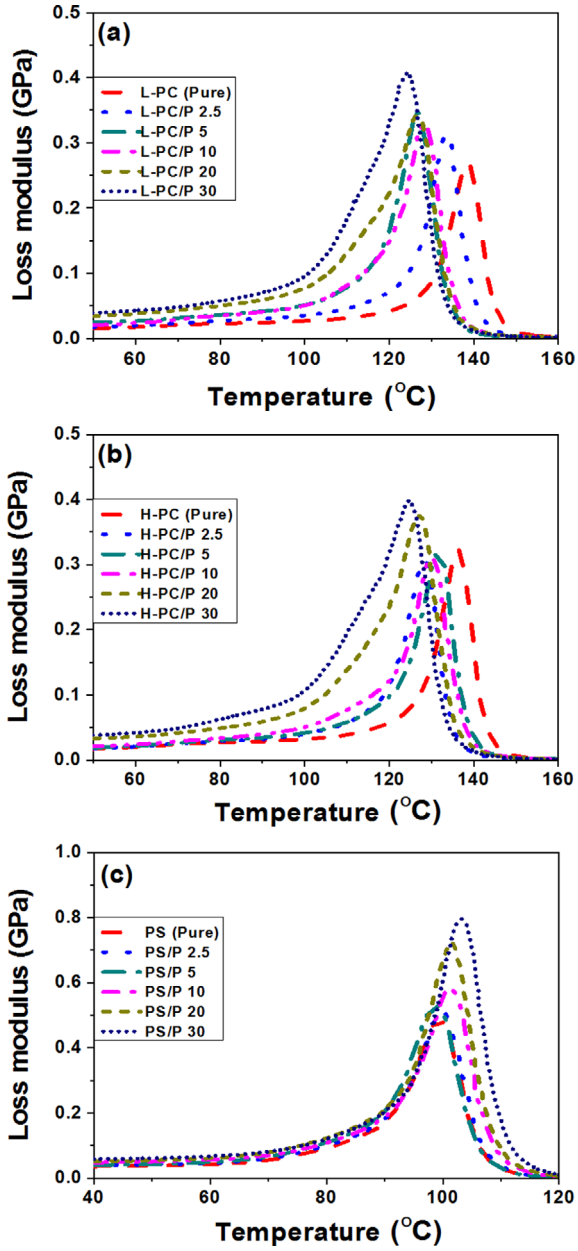


**Figure 8.** Loss moduli of phlogopite-incorporated (a) L-PC, (b) H-PC, and (c) PS composites with different phlogopite loadings.

increased with increasing filler content, which indicates that the viscous characteristics of the composites increased.

The tan $\delta$ ($E''/E'$) depends on the structural deformation of materials. The $T_g$ values can be determined by tan $\delta$. The $T_g$ of PC composites decreased with increasing phlogopite concentration because of chain scission of PC. In contrast, the incorporation of phlogopite into the PS matrix increased the $T_g$ of the composites owing to good interfacial interactions without PS polymer chain scission. The intensity of tan $\delta$ for both L-PC and H-PC composites decreased from 1.5 to 1.25 with increasing phlogopite content from 0 to 30 phr, indicating that the composites became more elastic characteristics owing to the incorporation of phlogopite. The width of tan $\delta$ curve increased as a function of phlogopite loading. The width of tan $\delta$ curve is correlated with relaxation of polymer chains. Due to the interfacial

**Table 1.** $T_g$ values of phlogopite-incorporated L-PC, H-PC, and PS composites with different phlogopite loadings (DSC, DMA)

| Phlogopite (phr) | L-PC | | H-PC | | PS | |
|---|---|---|---|---|---|---|
| | DSC | DMA | DSC | DMA | DSC | DMA |
| 0 | 145.1 | 143.5 | 144.5 | 141.7 | 103.7 | 107.3 |
| 2.5 | 139.9 | 139.5 | 139.9 | 133.9 | 103.9 | 106.9 |
| 5 | 138.7 | 133.3 | 139.9 | 137.7 | 104.1 | 106.3 |
| 10 | 135.6 | 135.4 | 138.2 | 137.4 | 103.9 | 108.7 |
| 20 | 134.0 | 134.2 | 134.5 | 134.9 | 104.6 | 108.8 |
| 30 | 135.2 | 133.0 | 135.5 | 133.1 | 104.3 | 110.3 |

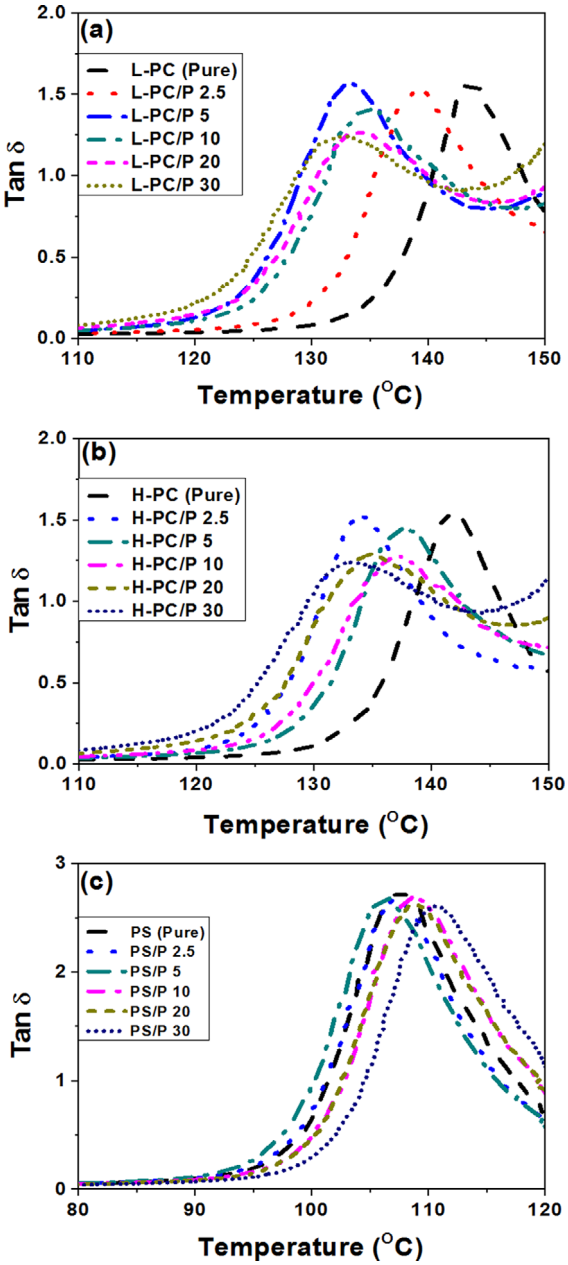


**Figure 9.** Tan $\delta$ of phlogopite-incorporated (a) L-PC, (b) H-PC, and (c) PS composites with different phlogopite loadings.

interactions between phlogopite surfaces and polymer chains, the molecular mobility of polymer chain was hindered, thereby resulting in the relaxation of polymer chains and broad peaks.

Figures 10(a) and 10(b) show the $T_g$ and degradation point ($T_d$) of L-PC, H-PC, and PS composites as a function of phlogopite concentration, respectively. The $T_g$ and $T_d$ of PS composites gradually increased as a function of phlogopite content owing to interfacial interactions between the PS chains and fillers. By contrast, the $T_g$ (Figure 10(a)) and $T_d$ (Figures 10(b) and S6) of L-PC and H-PC composites decreased with increasing filler content because the incorporation of phlogopite into the PC matrices resulted in PC chain scission despite interfacial interactions between the PC matrix and fillers, thereby reducing the MW of PC. Based on various mechanical properties, storage/loss moduli, and thermal properties, the reduction in MW may be the cause of reduction in various properties of PCs. The MWs of L-PC, H-PC, and PS were measured as shown in Figure 11. The MW of PS gradually increased as a function of phlogopite whereas that of L-PC and H-PC decreased, indicating the PC chain scission (especially carbonate group). The MW of PS slightly increased as a function of phlogopite loading probably because the PS archi-

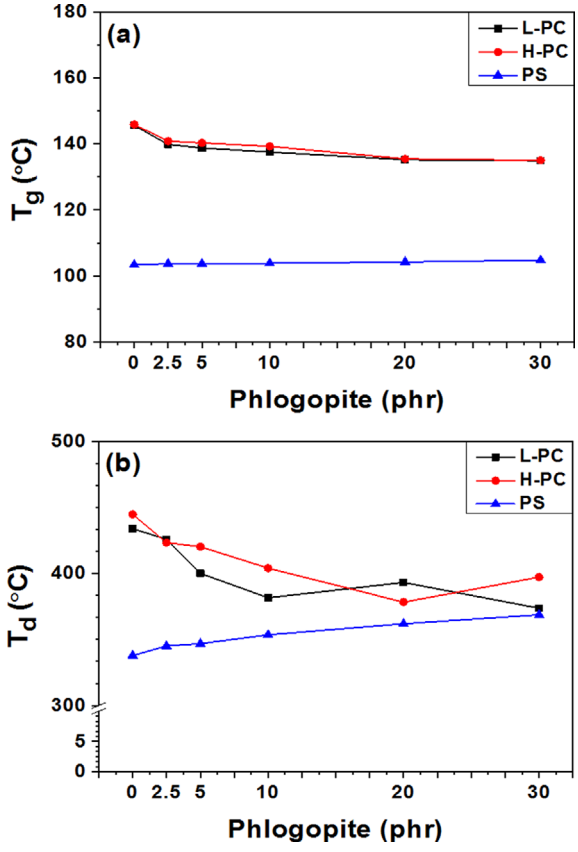


**Figure 10.** $T_g$ (a) and $T_d$ (b) of phlogopite-incorporated L-PC, H-PC, and PS composites with different phlogopite loadings.

 

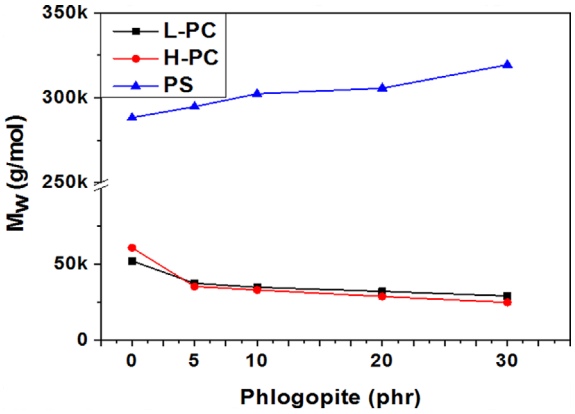


**Figure 11.** MWs of phlogopite-incorporated L-PC, H-PC, and PS composites with different phlogopite loadings.

tecture transitioned from random coil to rod-like conformation in solution, caused by the incorporation of phlogopite during extrusion. The MW of polymers is routinely determined by a relative MW measurement method, such as GPC. The rod-like architecture may have overestimated the MW of PS.[40-42] According to Flory-Fox equation,[43] the $T_g$ of a polymer is proportional to its MW.

The infiltration of phlogopite into the PC matrix significantly increased the melt flow index (MFI) of PC composites due to the PC chain scission as shown in Figure 12. The MFI of L-PC more substantially increased than that of H-PC. In contrast, the MFI of PS decreased due to the restricted PS chain flow caused by the filler. The MFI of a polymer and a polymeric composite is inversely proportional to its MW.

As discussed, the incorporation of phlogopite into the PC matrices decreased most of the mechanical and thermal properties. Thus, other common mineral fillers such as kaolin and silica (see the SEM images in Figure S7) were also utilized to compare the effects of filler types on the composite properties. The tensile test results of PC composites with filler contents of 10 phr are shown in Figure 13. The tensile strength of PC/kaolin composite slightly decreased from 58 to 50 MPa whereas that of PC/phlogopite and PC/silica substantially decreased, compared with the pristine PC matrix, as shown in Figure 13(a). Figure 13(b) shows that the elongation at break of all composites dramatically decreased due to the increased stress concentration caused by the incorporation of fillers in the PC matrix. By contrast, regardless of filler type, the tensile modulus of the PC composites was enhanced by the fillers (Figure 13(c)). In particular, the modulus of PC/phlogopite composites was the highest among other PC/filler composites. Similar to the results of elongation at break, the impact strengths of PC composites were considerably reduced by the filler infiltration (Figure 14). Based on the mechanical tests of PC composites, the effect of phlogopite on mechanical properties was analogous to that of other common fillers except for the tensile modulus. The phlogopite for PC exhibited the most significant effect on the tensile modulus among PC/filler composites.

Thermal properties ($T_g$ and $T_d$) of PC composites with differ-

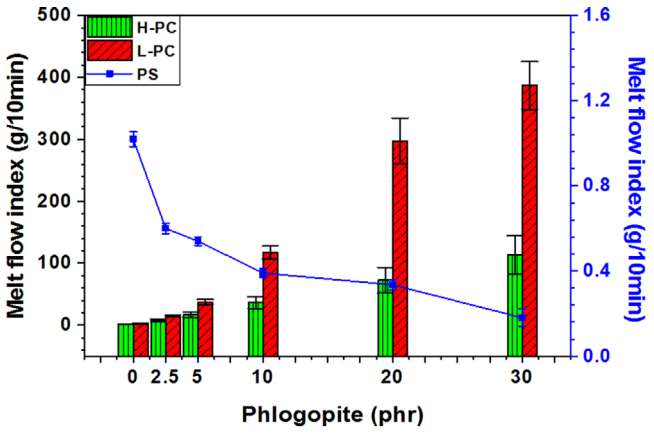


**Figure 12.** MFIs of phlogopite-incorporated L-PC, H-PC, and PS composites with different phlogopite loadings.

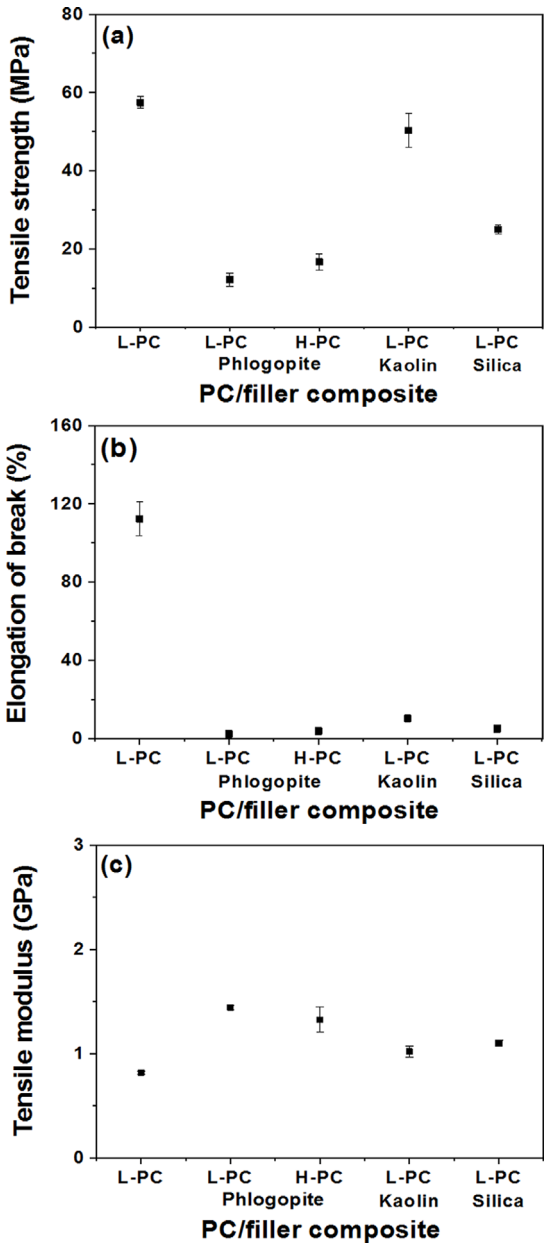


**Figure 13.** Tensile tests of L-PC and H-PC composites with different fillers (phlogopite, kaolin, and silica) with 10 phr filler: (a) tensile strength, (b) elongation at break, and (c) modulus.

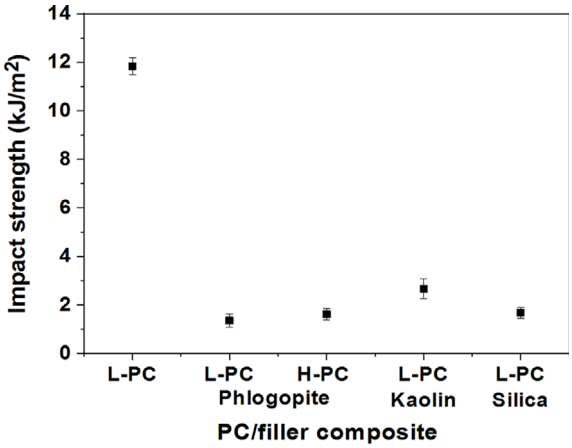


**Figure 14.** Impact strength of L-PC and H-PC composites with different fillers (phlogopite, kaolin, and silica) at 10 phr filler.

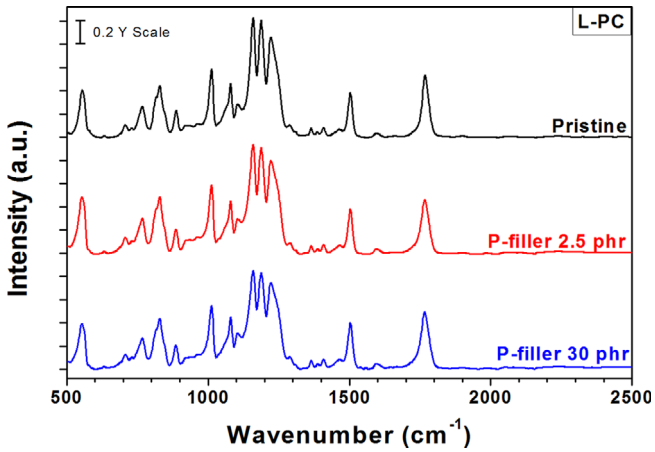


**Figure 16.** FTIR spectra of L-PC/phlogopite composites with different filler content.

ent mineral fillers were examined, as shown in Figures 15, S8, and S9. The trend for $T_g$ values of PC composites was analogous to that for $T_d$ values. The incorporation of all fillers into the PC matrices reduced the $T_g$ and $T_d$ values because of the ductile-to-brittle transition[44] caused by the increase in stress concentration.[45] The $T_g$ and $T_d$ values of PC/phlogopite composites were lower than those of PC/silica and PC/kaolin composites although the tensile modulus of PC/phlogopite composites was the highest. The other mechanical properties of PC/phlogopite composites were the lowest. The modulus is typically determined by the interfacial adhesion (interaction) between the filler and matrix. Thus, the results of mechanical and thermal properties of PC/filler composites indicate that the interfacial interactions between the phlogopite and PC were the highest whereas the incorporation of phlogopite into the PC matrix resulted in the most PC chain scission, thereby representing the greatest decrease in the MW of PCs. Figure 16 shows FTIR spectra of L-PC/phlogopite composites with different phlogopite concentrations. The peak at 1250-1150 $cm^{-1}$ ascribed to C-O in carbonate groups decreased with increasing phlogopite content. This indicates that the phlogopite attacked the carbonate groups, thereby decreasing MW and properties of PC.

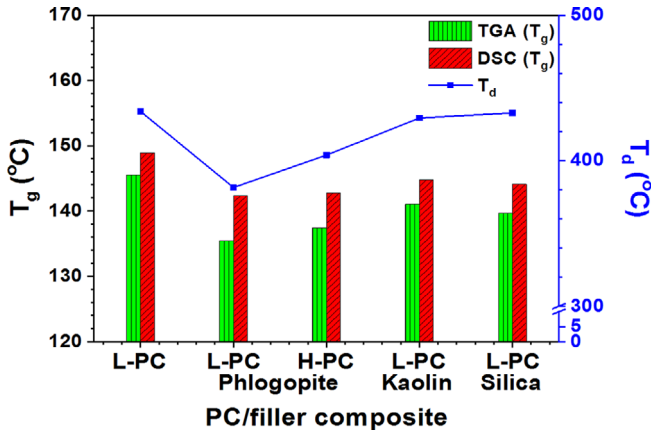


**Figure 15.** $T_g$ (a) and $T_d$ (b) of L-PC and H-PC composites with different fillers (phlogopite, kaolin, and silica) at 10 phr filler.

## 4. Conclusion

The mechanical, thermal, and rheological properties of phlogopite-embedded PC and PS composites were explored in this study. The mechanical (strength, modulus, elongation at break, impact strength, and storage/loss moduli) and thermal ($T_g$ and $T_d$) properties of phlogopite-reinforced PS composites were enhanced as a function of phlogopite loading. By contrast, most properties of phlogopite-embedded PC decreased except the tensile modulus with increasing phlogopite concentration. The moduli of PC/phlogopite composites were the highest among other PC/filler composites. The mechanical and thermal properties of PC/filler composites were determined by the competition between the PC chain scission (reduction in MW) caused by fillers and the interfacial interaction between the PC and fillers. Kaolin and silica were employed for comparison with the phlogopite.

**Acknowledgement:** This work was supported by the Technology Innovation Program (or Industrial Strategic Technology Development Program-Material Components Technology Development Program) (No. 20011433, Extremely cold-resistant anti-vibration elastomer with EPDM) funded by the Ministry of Trade, Industry & Energy (MOTIE, Korea). This work was supported by the National Research Foundation of Korea (NRF) grant funded by the Korea government (MSIT) (No. 2021R1G1A1011525, Rapid low-temperature curing of thermoset resins via microwave). This work was supported by the Technology Innovation Program (or Industrial Strategic Technology Development Program- Nano fusion innovative product technology development) (No. 20014475, Anti-fog nano-composite-based head lamp with <10% of low moisture adsorption in surface area) funded By the Ministry of Trade, Industry & Energy (MOTIE, Korea). This work was supported by the Technology Innovation Program (or Industrial Strategic Technology Development Program- Automobile industry technology development) (20015803, High performance composite-based battery pack case for electric vehicles via hybrid structure and weight lightening technology) funded By the Ministry of Trade, Industry & Energy (MOTIE, Korea).

 

This work was supported by the Technology development Program (Antistatic extrudable carbon nanotube/polymer composites with $10^6$-$10^8$ ohm/sq of surface resistance for display tray: S3111196) funded by the Ministry of SMEs and Startups (MSS, Korea). This work was supported by the INNOPOLIS Foundation grant funded by the Korea government (MSIT) (Development of sintered Cu bonding material with Pb-free for power semiconductor module: 2021-DD-RD-0385-01). This research was supported by Research and Business Development Program through the Korea Institute for Advancement of Technology (KIAT) funded by the Ministry of Trade, Industry and Energy (MOTIE) (Development of one step black epoxy bonding film for micro LED display, grant number: P0018198). This research was also supported by Advanced Materials Analysis Center, The University of Suwon). This research was supported by Basic Science Research Program through the National Research Foundation of Korea (NRF) funded by the Ministry of Education, Science and Technology (NRF-2019R1I1A2A01051610).

**Supporting information:** Figure S1: SEM images of pure H-PC and H-PC/P composites with different phlogopite concentrations: (a) Pure H-PC, (b) H-PC/P2.5, (c) H-PC/P5, (d) H-PC/P10, (e) H-PC/P20, and (f) H-PC/P30, Figure S2: SEM images of H-PC/P, L-PC/P and PS/P composites with different phlogopite concentrations: (a) L-PC/P, (b) H-PC/P, and (c) PS/P, Figure S3: Stress-strain curves of L-PC, H-PC, and PS composites with different phlogopite contents, Figure S4: (a) SEM images of phlogopite, (b) histogram of phlogopite dimensions, and (c) major and minor axises, Figure S5: DSC scans of phlogopite-incorporated L-PC (a), H-PC (b), and PS (c) composites with different phlogopite loadings, Figure S6: TGA scans of phlogopite-incorporated L-PC (a), H-PC (b), and PS (c) composites with different phlogopite loadings, Figure S7: SEM images: (a) phlogopite, (b) kaolin, and (c) silica, Figure S8: DSC scans of L-PC and H-PC composites with different fillers (phlogopite, kaolin, and silica) with 10 phr filler, Figure S9: TGA scans of L-PC and H-PC composites with different fillers (phlogopite, kaolin, and silica) with 10 phr filler. The materials are available *via* the Internet at http://www.springer.com/13233.

## References

(1) M. Miyashita, and M. Yamaguchi, *Polymer*, **202**, 122713 (2020).
(2) Y. T. Sung, M. S. Han, K. H. Song, J. W. Jung, H. S. Lee, C. K. Kum, J. Joo, and W. N. Kim, *Polymer,* **47**, 4434 (2006).
(3) K. S. Jang, *Polymer.,* **147**, 133 (2018).
(4) T. W. Cheng, H. Keskkula, and D. R. Paul, *Polymer,* **33**, 1606 (1992).
(5) N. Hasegawa, H. Okamoto, M. Kawasumi, and A. Usuki, *J. Appl. Polym. Sci.,* **74**, 3359 (1999).
(6) Z. Yang, B. Dong, Y. Huang, L. Liu, F.-Y. Yan, and H.-L. Li, *Mater. Chem. Phys.,* **94**, 109 (2005).
(7) V. Abdelsayed, E. Alsharaeh, and M. S. El-Shall, *J. Phys. Chem. B*, **110**, 19100 (2006).
(8) K. S. Jang, *Polym Test.,* **84**, 106408 (2020).
(9) K. S. Jang, *E-Polymers,* **16**, 379 (2016).
(10) O. Bera, B. Pilić, J. Pavličević, M. Jovičić, B. Holló, K. M. Szécsényi, and M. Špirkova, *Thermochim. Acta,* **515**, 1 (2011).
(11) J. L. H. Chau, S. L.-C. Hsu, Y.-M. Chen, C.-C. Yang, and P. C. F. Hsu, *Adv. Powder Technol.,* **21**, 341 (2010).
(12) Y. Imai, A. Terahara, Y. Hakuta, K. Matsui, H. Hayashi, and N. Ueno, *Eur. Polym. J.,* **45**, 630 (2009).
(13) F. J. Carrión, J. Sanes, and M.-D. Bermúdez, *Wear.,* **262**, 1504 (2007).
(14) S. Thomas, in *Polymer Composites, Macro-and Microcomposites*, K. Joseph, S. K. Malhotra, K. Goda, and M. S. Sreekala, Eds., Wiley-VCH, German, 2012, pp 673-713.
(15) B. Diawara, K. Fatyeyeva, J. Ortiz, and S. Marais, *Polymer*, **230**, 124030 (2021).
(16) F. Asyadi, M. Jawaid, A. Hassan, and M. U. Wahit, *Polym. Plast. Technol. Eng.,* **52**, 727 (2013).
(17) J. W. Anthony, in *Handbook of Mineralogy*, R. A. Bideaux, K. W. Bladh, and M. C. Nichols, Eds., Mineralogical Society of America, Chantilly, 2003, pp 2870-2871.
(18) M. DeSarkar, P. Senthilkumar, S. Franklin, and G. Chatterjee, *J. Appl. Polym. Sci.,* **124**, 215 (2012).
(19) H. Zeng, J. Huang, Y. Tian, L. Li, M. V. Tirrell, and J. N. Israelachvili, *Macromolecules,* **49**, 5223 (2016).
(20) H. Y. Cheng, G. J. Jiang, J. Y. Hung, *Polym. Compos.,* **30**, 351 (2009).
(21) J. E. Kogel, in *Industrial Minerals & Rocks: Commodities, Markets, and Uses,* N. C. Trivedi, J. M. Barker, and S. T. Krukowski, Eds., Society for Mining, Metallurgy, and Exploration, USA, 2006, pp 637-652.
(22) C. J. R. Verbeek, *Mater. Lett.,* **52**, 453 (2002).
(23) L. Cai and Q. Dou, *Polym. Compos.,* **40**, E795 (2019).
(24) V. B. Chalivendra, *J. Mater. Sci.,* **38**, 1631 (2003).
(25) A. Davis, J. H. Golden, *Makromol. Chem.,* **78**, 16 (1964).
(26) C. Bailly, M. Daumerie, R. Legras, and J. P. Mercier, *Makromol. Chem.*, **187**, 1197 (1986).
(27) I. C. McNeill and A. Rincon, *Polym. Degrad. Stab.*, **39**, 13 (1993).
(28) A. Factor, *Angew. Makromol. Chem.,* **232**, 27 (1995).
(29) C. Puglisi, L. Sturiale, and G. Montaudo, *Macromolecules*, **32**, 2194 (1999).
(30) H. Jiang, J. Zhang, Z. Yang, C. Jiang, and G. Kang, *Int. J. Solids Struct.,* **124**, 215 (2017).
(31) A. Davis and J. H. Golden, *Nature,* **206**, 397 (1965).
(32) A. Davis and J. H. Golden, *J. Chem. Soc. B: Phys. Org.*, 45 (1968).
(33) K. B. Abbås, *Polymer,* **21**, 936 (1980).
(34) K. B. Abbås, *Polymer,* **22**, 836 (1981).
(35) J. C. Halpin, *J. Compos. Mater.,* **3**, 732 (1969).
(36) E. Guth, *Rubber Chem. Technol.,* **18**, 596 (1945).
(37) S. Wolff and J.-B. Donnet, *Rubber Chem. Technol.,* **63**, 32 (1990).
(38) Y. Seong, H. Lee, S. Kim, C. H. Yun, C. Park, C. Nah, and G.-B. Lee, *Elastom. Compos.*, **55**, 306 (2020).
(39) K. Jang, *J. Appl. Polym. Sci.,* **136**, 47110 (2019).
(40) S. Holdcroft, *J. Polym. Sci. B: Polym. Phys.,* **29**, 1585 (1991).
(41) K. S. Jang, Y. S. Eom, T. W. Lee, D. O. Kim, Y. S. Oh, H. C. Jung, and J. D. Nam, *ACS Appl. Mater. Interfaces,* **1**, 1567 (2009).
(42) J. Liu, R. S. Loewe, and R. D. McCullough, *Macromolecules*, **32**, 5777 (1999).
(43) T. G. Fox and P. J. Flory, *J. Appl. Phys.*, **21**, 581 (1950).
(44) D. G. Legrand, *J. Appl. Polym. Sci.*, **13**, 2129 (1969).
(45) B. K. Satapathy, R. Weidisch, P. Pötschke, and A. Janke, *Compos. Sci. Technol.*, **67**, 867 (2007).